Tuning the Electronic Properties of Semiconducting Transition Metal Dichalcogenides by Applying Mechanical Strains

Priya Johari* **and Vivek B. Shenoy***

School of Engineering, Brown University, Providence, Rhode Island 02906, United States

ABSTRACT Semiconducting transition metal dichalcogenides (TMDs) are emerging as the potential alternatives to graphene. As in the case of graphene, the monolayer of TMDs can easily be exfoliated using mechanical or chemical methods, and their properties can also be tuned. At the same time, semiconducting TMDs (MX_2; M = Mo, W and X = S, Se, Te) possess an advantage over graphene in that they exhibit a band gap whose magnitude is appropriate for applications in the optoelectronic devices. Using *ab initio* simulations, we demonstrate that this band gap can be widely tuned by applying mechanical strains. While the electronic properties of graphene remain almost unaffected by tensile strains, we find TMDs to be sensitive to both tensile and shear strains. Moreover, compared to that of graphene, a much smaller amount of strain is required to vary the band gap of TMDs. Our results suggest that mechanical strains reduce the band gap of semiconducting TMDs causing an direct-to-indirect band gap and a semiconductor-to-metal transition. These transitions, however, significantly depend on the type of applied strain and the type of chalcogenide atoms. The diffuse nature of heavier chalcogenides require relatively more tensile and less shear strain (when the monolayer is expanded in *y*-direction and compressed in *x*-direction) to attain a direct-to-indirect band gap transition. In addition, our results demonstrate that the homogeneous biaxial tensile strain of around 10% leads to semiconductor-to-metal transition in all semiconducting TMDs, while through pure shear strain this transition can only be achieved by expanding and compressing the monolayer of MTe_2 in the *y*- and *x*-directions, respectively. Our results highlight the importance of tensile and pure shear strains in tuning the electronic properties of TMDs by illustrating a substantial impact of the strain on going from MS_2 to MSe_2 to MTe_2.

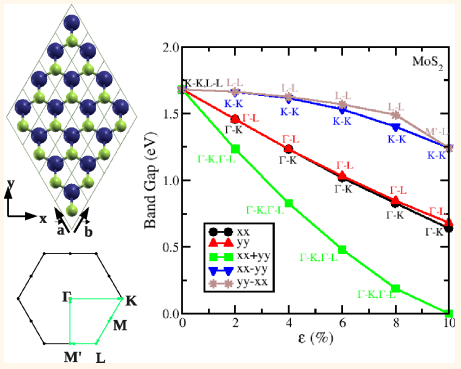

KEYWORDS: 2D materials · diachalcogenides · DFT

Transition metal dichalcogenides (TMDs) which belong to the family of layered materials, classify a broad spectrum of materials ranging from insulators to semiconductors to semimetals to metals. They, thus, find applications in various fields such as opto-electronics, photovoltaics, batteries, defense, space, *etc.*[1−11] TMDs exhibit a "sandwich" type of structure (X−M−X) in which metal atoms (M) are located in between two layers of chalcogen atoms (X) (see Figure 1). Atoms within these three layers are bonded covalently, while individual sheets are bound *via* weak van der Waals interaction, which makes the properties of these materials extremely anisotropic. Similar to graphene, single sheets of TMDs can be extracted from the bulk using mechanical or solvent-based-exfoliation methods.[8−11] However, unlike graphene, which is intricate to use in opto-electronic devices due to its zero band gap, the semiconducting TMDs (MoX_2 and WX_2; X = S, Se, and Te) possess a band gap suitable for device applications. Owing to strong surface effects, the properties of these materials vary drastically with the number of layers in a sheet. Therefore, they can be tuned on demand, which makes them a potential candidate for tunable nano-electronics. For example, (a) the electron energy loss spectra of TMDs shifts toward larger wavelengths (red shift) with the decrease in number of layers,[12] (b) the band gap increases from multilayer-to-single layer, and (c) multilayer MoX_2 and WX_2 are indirect band gap semiconductors, while their monolayers exhibit direct band gap. Monolayer MoX_2 and WX_2 can complement graphene in the applications that require thin transparent semiconductors, such as opto-electronics and energy harvesting. Being a direct band gap semiconductor, they can also be used to construct interband tunnel FETs.[11,13,14] Recently, a field effect transistor with a mobility rate comparable to silicon and graphene nanoribbons (200 $cm^2 V^{-1} s^{-1}$), high room temperature current on/off ratios, and ultralow standby power dissipation has been demonstrated using single layer MoS_2.[11] Moreover, the ultrathin films of TMDs are also promising for obtaining nanotubes and other nanomaterials which show confinement effects in their electronic and optical properties. On the other hand, indirect semiconducting TMDs (thicker films or bulk) hold promise in photovoltaic applications such as electrodes in high-efficiency photochemical

* Address correspondence to psony11@gmail.com, Vivek_Shenoy@brown.edu.

Received for review March 25, 2012 and accepted May 16, 2012.

Published online May 16, 2012
10.1021/nn301320r

cells, as their optical band gap is comparable to the solar wavelength.[15−19]

The properties of TMDs cannot only be tuned by varying the number of layers, but can also be modified by nanopatterning, chemical treatment, application of an external electric field or strain engineering. Nanopatterning and chemical treatment, however, can damage the 2D sheet and induce disorders, which can deterioriate the performance of the devices in terms of charge transport. Similar to graphene, the band gap of a single layer of semiconducting TMDs remains uneffected by the external electric field and can only be modulated when there are two or more layers.[20] Thus, all of the above-discussed schemes allow for tuning of the band gap but possess limitations in their own ways. Recently, strain engineering was identified as one of the best possible strategies to tune the band gap, since it neither attenuates the properties nor is inefficacious for single layers.[21,22] The strain can be induced easily by growing the TMDs on flexible substrates.[23,24] Thus, by applying strain, features similar to nanopatterning and chemical treatment can be obtained, without permanent effect on the 2D sheet, as this process is fully reversible.

So far, strain engineering has proved to be an efficient way to induce and tune the band gap in graphene. It has been demonstrated both experimentally and theoretically that the optical, phononic, and electronic properties of graphene can be tuned and controlled by varying the strain from ∼12% to 20%.[22,23,25,26] This variation however strongly depends on the direction of the applied strain, as the band gap of graphene remains robust against uniaxial and symmetrical biaxial tensile strain,[24,25,27] and varies only when shear or a combination of shear and uniaxial deformation is applied. The monolayer of semiconducting TMDs already exhibits a direct band gap ranging approximately from 1.81 to 1.06 eV.[17,28] However, if this band gap can be tuned such that a semiconductor with a lower band gap or a semiconductor-to-metal transition can be achieved with the application of strain, then a wide range of tunable nanodevices can be fabricated. In the present work, therefore, we study the effect of mechanical strains on the electronic properties of monolayers of several semiconducting TMDs such as MoS_2, $MoSe_2$, $MoTe_2$, WS_2, WSe_2, and WTe_2. To this extent, we applied tensile as well as pure shear strain (expansion in one direction and compression in another) to the monolayers in the direction parallel to the basal plane and computed their electronic structure using first-principles density-functional-theory (DFT) based methodology. The effect of homogeneous biaxial tensile strain on semiconducting TMDs has been very recently studied.[28,29] However, to the best of our knowledge, strain profiles other than symmetrical biaxial tensile and compressive strains, have not been considered in any of the previous theoretical investigations for TMDs. Thus, by considering various strain profiles including uniaxial and biaxial tensile strain, and pure shear strain, our calculations cover a broader aspect of strain engineering and provide a mechanical pathway to substantially engineer the electronic properties of TMDs.

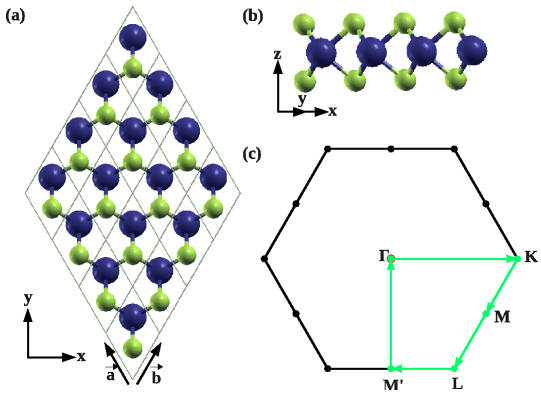

Figure 1. (a) Top and (b) side view of MX_2, where big and small spheres depict M and X atoms, respectively. The figure shows a 4 × 4 supercell, where each of the unit cell is represented by gray (dashed) boxes. The symbols $\vec{a}$ and $\vec{b}$ symbolize the in-plane lattice vectors, which are defined as $[0.5a, -0.5\sqrt{3}a, 0]$ and $[0.5a, 0.5\sqrt{3}a, 0]$, respectively, where a is the lattice constant of MX_2. The strain along x or/and y-directions is applied by varying the x or/and y components of these lattice vectors, respectively. (c) Irreducible Brillouin zone of MX_2. The irreducible path ΓKMΓ corresponds to the unstrained and symmetrically strained TMDs, while ΓKMLM′Γ encloses the irreducible wedge for the asymmetrically strained TMDs.

RESULTS AND DISCUSSION

To study the effect of strain on the electronic properties of semiconducting TMDs, we first relaxed the atomic positions as well as lattice vectors and obtained the optimized geometry of monolayer MX_2 (M = Mo and W; X = S, Se, and Te). The optimized value of lattice constant a_0 is found to be 3.18 Å (MoS_2), 3.32 Å ($MoSe_2$), 3.55 Å ($MoTe_2$), 3.18 Å (WS_2), 3.31 Å (WSe_2), and 3.55 Å (WTe_2). The value of a_0 increases going from S to Se to Te, while it remains the same with the change in transition metal, that is, $a_0(MoX_2) \simeq a_0(WX_2)$. The strained cell is modeled by stretching/compressing the hexagonal ring in the x- or/and y-directions. The top and side views of generalized structure of semiconducting TMDs with hexagonal symmetry and its irreducible Brillouin zone are illustrated in Figure 1. The band structure is calculated along high symmetry points Γ, K, M, L, M′ as depicted in Figure 1c. The irreducible path ΓKMΓ corresponds to the unstrained and symmetrically strained TMDs, while ΓKMLM′Γ encloses the irreducible wedge for the asymmetrically strained TMDs. Thus, for symmetrical systems K(M) and L(M′) points are identical.

On calculating the band structure of unstrained monolayer MX_2, we find that all the investigated systems exhibit a direct band gap with valence band

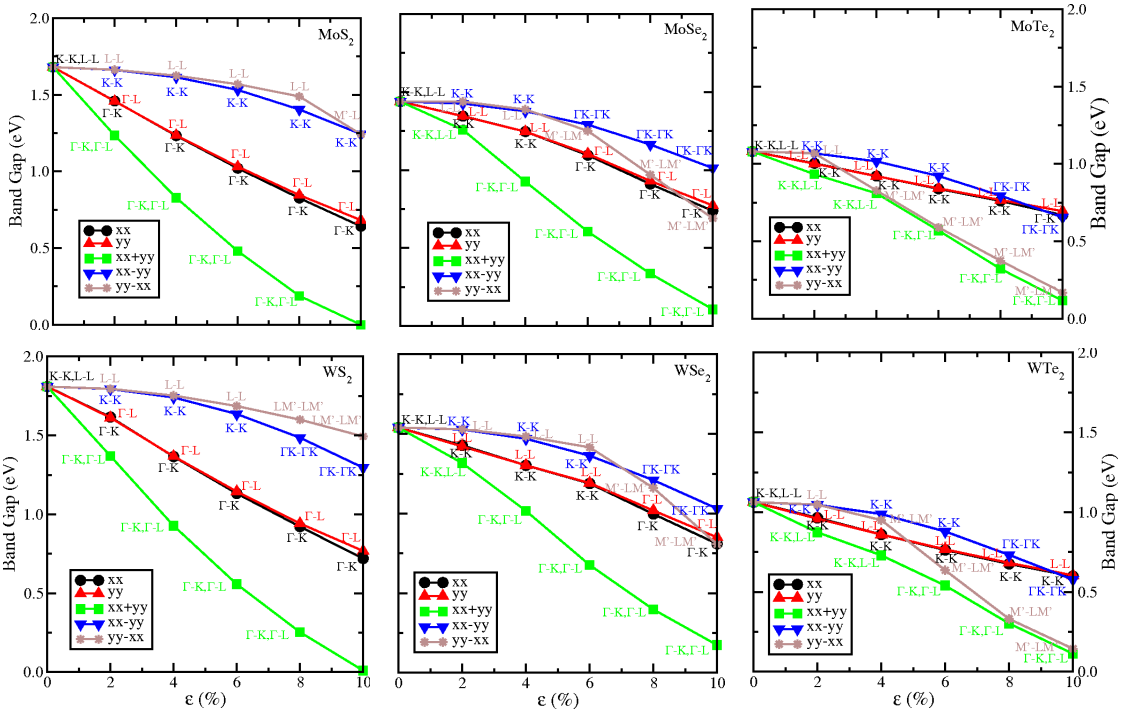

Figure 2. Band gap of monolayer TMDs with respect to strain, ε, which varies from 0 to 10%. Strain is applied to the optimized structures ($\varepsilon = 0$) through various approaches, such as uniaxial expansion in *x*-direction (*xx*), *y*-direction (*yy*), homogeneous expansion in both *x*- and *y*-directions (*xx*+*yy*), expansion in *x*-direction and compression in *y*-direction (*xx*−*yy*), and compression in *x*-direction and expansion in *y*-direction (*yy*−*xx*) with same magnitude of strain. The first three strain profiles correspond to tensile strain, while the latter two represent pure shear strain. The top (left, middle, and right) panels of Figure 2 depict the graphs corresponding to MoX_2 (WX_2), while the bottom panels show the same for MS_2, MSe_2, and MTe_2, respectively, where M denotes Mo or W.

maximum (VBM) and conduction band minimum (CBM) located at the high symmetry point K. We calculate the band gap of optimized monolayer MoS_2, $MoSe_2$, $MoTe_2$, WS_2, WSe_2, and WTe_2 to be 1.68, 1.44, 1.08, 1.81, 1.54, and 1.06 eV, respectively. It is well-known that the semilocal functionals in DFT underestimate the band gap, while hybrid functionals that have a certain percentage of Hartree−Fock exchange or the many-body techniques generally lead to better agreement with experiments. However, this trend is not generalized, and more often depends on the material considered. For example, our calculated PBE band gap for monolayer MoS_2 underestimates the experimental band gap of 1.8 eV by just 0.12 eV.[30] Recently, Kuc *et al.*[31] and Ataca and Ciraci[32] showed that PBE0 and HSE06 hybrid functionals overestimate this band gap by approximately 1 and 0.45 eV, respectively. Moreover, Ataca and Ciraci[32] also reported a higher value of the band gap (G_0W_0 gap of 2.78 eV and GW_0 gap of 2.5 eV) obtained using many-body GW methods. Analyzing the aforementioned data, we believe that our choice of the PBE exchange-correlation functional for current systems is appropriate, and a general idea of the trends can be anticipated from our results.

We next present the band gaps of symmetrically and asymmetrically strained monolayer TMDs. As mentioned above, tensile and pure shear strains are applied to the optimized structures through various approaches to study the effect of mechanical strains on the electronic properties of semiconducting TMDs. The tensile strain is realized in three different ways: uniaxial expansion of monolayer in *x*-direction (*xx*), *y*-direction (*yy*), and homogeneous biaxial expansion in both *x*- and *y*-directions (*xx*+*yy*), while two types of pure shear strain are applied by expanding and compressing the monolayer in *x*- and *y*-directions (*xx*−*yy*), respectively, and by compressing it in *x*-direction and expanding in *y*-direction (*yy*−*xx*) with the same magnitude of strain. Figure 2 presents the band gaps of monolayer MX_2 with respect to strain, applied using the above-mentioned approaches. The top (bottom) panel of Figure 2 depicts the graphs corresponding to MoX_2 (WX_2), while the left, middle, and right panels show the same for MS_2, MSe_2, and MTe_2, respectively, where M denotes Mo or W. It is evident from Figure 2 that the variations in the band gap with respect to strain applied through various approaches do not alter much with the change in transition metal, Mo and W. However, a qualitative as well as quantitative diversity in the trends can be seen with the change in chalcogenides, while moving from MS_2 to MSe_2 to MTe_2.

Starting with the lighter compounds, that is, MS_2, we investigate the variation in the nature of the band gap for MS_2 upon application of tensile strain and report a monotonic decrease of the band gap with strain.

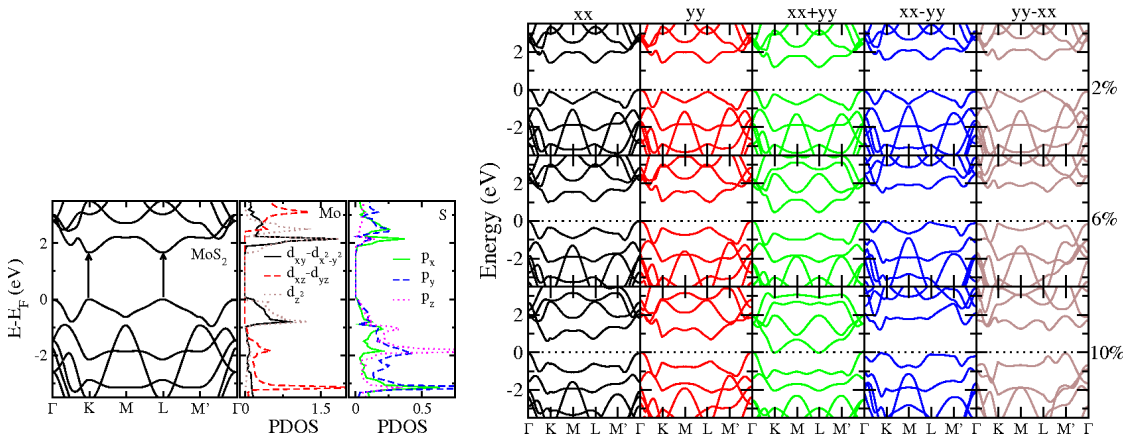

Figure 3. Left panel: Band structure and PDOS of unstrained MoS_2. Right panel: Band structures of MoS_2 corresponding to ε = 2%, 6%, and 10%, when strain is applied to the optimized structures (ε = 0) through various approaches, such as uniaxial expansion in *x*-direction (*xx*), *y*-direction (*yy*), homogeneous expansion in both *x*- and *y*-directions (*xx*+*yy*), expansion in *x*-direction and compression in *y*-direction (*xx*−*yy*), and compression in *x*-direction and expansion in *y*-direction (*yy*−*xx*) with same magnitude of strain.

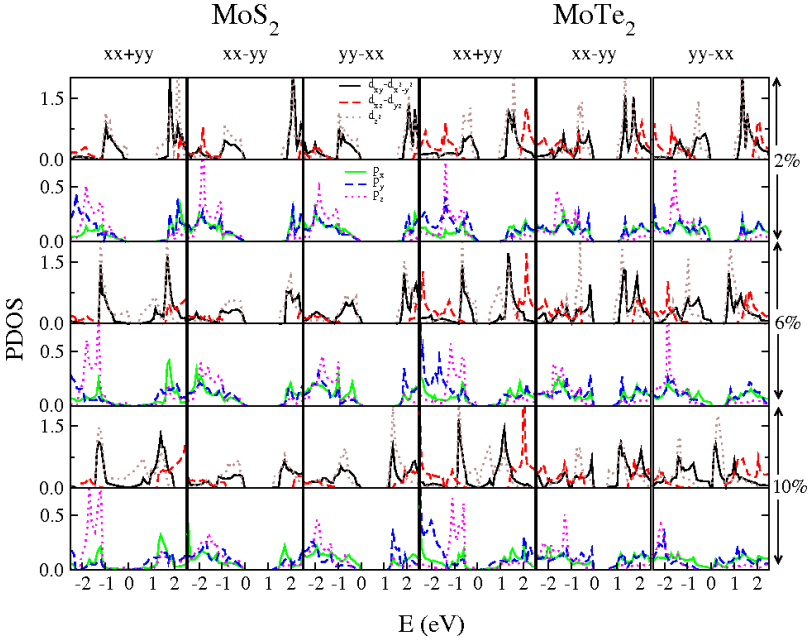

Figure 4. PDOS of MoS_2 and $MoTe_2$ when the monolayers are stretched in both *x*- and *y*-directions (*xx*+*yy*), expanded along the *x*/*y*-direction and compressed along the *y*/*x*-direction (*xx*−*yy*/*yy*−*xx*) with 2%, 6%, and 10% strain. Moving from top to bottom, alternate rows depict PDOS of p- and d-orbitals, respectively.

In particular, upon application of tensile strain, the shortest transition that was otherwise a direct band transition for the unstrained system, transforms to an indirect band transition which corresponds to (i) Γ−K, when the monolayer is stretched in *x*-direction; (ii) Γ−L, when it is stretched in *y*-direction; and (iii) Γ−K and Γ−L, when the sheet is homogeneously stretched in both *x*- and *y*-directions (see left portion of Figure 2). To understand this transition, we analyze the band structure and partial density of states (PDOS) of unstrained (see the left panel of Figure 3) and strained monolayer of MoS_2 (see the right panel of Figure 3 and Figure 4). For better visibility we present band structure and PDOS of some selected cases only. For example, the right panel of Figure 3 shows the band structures of MoS_2 corresponding to all cases of strain, when the monolayer is deformed by 2%, 6%, and 10%, while Figure 4 depicts the PDOS of monolayer of MoS_2 and $MoTe_2$ corresponding to symmetrical biaxial tensile strain (*xx*+*yy*) and both cases of pure shear strain (*xx*−*yy* and *yy*−*xx*).

The left panel of Figure 3 shows that in the unstrained monolayer of MoS_2 the direct band gap corresponds to transition from the valence band maximum (VBM) to conduction band minimum (CBM) at K point of the Brillouin zone, where the VBM and CBM are mainly described by $d_{xy}-d_{x^2-y^2}$ and d_{z^2} orbitals, respectively. An examination of the band structure of strained MoS_2 (see the right panel of Figure 3)shows

that application of tensile strain (*xx*, *yy*, *xx*+*yy*) results in downward shifting of the valence band around K and L points, but does not affect the Γ point. This causes a shift in VBM from K and L points to Γ point, which is mainly described by the d_{z^2} orbital (see Figure 4), instead of the $d_{xy}-d_{x^2-y^2}$ orbitals. As the CBM around the K and L points does not experience a similar shift and on the contrary remains totally unaffected by the tensile strain, a direct-to-indirect band gap transformation occurs, attributing new electronic properties to the material. Moreover, the CBM at K (*xx*), L (*yy*) and both K and L (*xx*+*yy*) points shift toward the Fermi level. This shift is relatively fast in the case of symmetrical biaxial tensile strain, leading to semiconductor-to-metal transformation at only 10% of strain. Our results are in perfect agreement with the recent calculations of Scalise *et al.*,[29] who discuss the change in electronic properties of monolayer MoS_2 from semiconducting to metallic when a symmetrical biaxial tensile (compressive) strain of 10% (15%) or more is applied. In the case of uniaxial expansion along *x*- and *y*-directions, our calculations predict that the band gap for both the cases (*xx* and *yy*) reduces concurrently with strain, resulting in approximately half the value of an unstrained system when the 2D sheet is stretched by 10% (see Figure 3 and Figure 2). These results are in contrast to what has been reported for graphene, where tensile strain only shifts the position of the Dirac cone and induces the band gap for strains higher than 20% .[25,27]

Besides tensile strain, shear strain is also responsible for band gap modifications, although here the band gap decrease for *xx*−*yy* and *yy*−*xx* is not as steep as for the case of tensile strain. For these examples of shear strain, the direct band gap character is retained for up to $\varepsilon = 10\%$ with the shortest transition corresponding to K−K (L−L). As for the case of tensile strain, we find that pure shear strain results in a shift of the CBM at K or/and L toward the Fermi level, but conversely, the VBM remains almost intact at K and L points, while the energy of the valence band at Γ point moves down (see Figure 3). This keeps the nature of the band gap consistent with the unstrained case. Moreover, similar to unstrained MoS_2, the VBM and the CBM are also described by $d_{xy}-d_{x^2-y^2}$ and d_{z^2} orbitals, respectively, in the case of pure shear strain. It is, however, noticed that when MoS_2 is expanded along the *y*-direction and compressed along the *x*-direction by 10% or more, the p_x orbital also contributes in defining the VBM (see Figure 4). This shifts the position of VBM from the L to M′ point of the irreducible Brillouin zone and leads to direct-to-indirect band gap transition. In the case of WS_2, no such transformation is seen until 10% of strain. However, with the increase in strain (>6%), the direct band gap transition shifts between Γ and K points when the surface is stretched in the *x*-direction and compressed in the *y*-direction, and between L and M′ high symmetry points when expansion and contraction are applied along the *y*- and *x*-directions, respectively (see Figure 2), due to an increase in the overlapping of d-orbitals of heavier metal.

So far, our results have underscored the importance of both tensile and shear strains on the electronic porperties of monolayers of the lighter TMDs, for example, MS_2. However, on examining TMDs exhibiting atoms heavier than S, such as Se and Te, we find that the diffuse nature of these chalcogenide atoms significantly affects their response to strain. Our results demonstrate that for MSe_2 and MTe_2, the band gap decreases relatively slow and larger amounts of tensile strain are required to obtain direct-to-indirect band transition (see from left to right in Figure 2). We observe that the direct-to-indirect band gap transition takes place when the tensile strain during biaxial straining of MSe_2 (MTe_2) is approximately two (four) times more than that of MS_2. On the application of uniaxial strain, MSe_2 (MTe_2) undergoes an even larger expansion, 4−6% (8−10%), in order to achieve the aforementioned transition.

Upon investigating the effect of shear strain, we find that in contrast to MS_2, where direct-to-indirect band gap transformation is not seen on the application of both types of discussed shear strain (until ∼10%), in MSe_2 and MTe_2, the expansion in the *y*-direction and compression in *x*-direction (*yy*−*xx*) leads to direct-to-indirect band gap transformation. This transition which corresponds to M′−LM′ is achieved faster, that is, at low strain (>2%) in MTe_2 as compared to that of MSe_2, where strain of more than 4−6% is required to change the nature of the band gap. The system, however, remains unaffected, and this transition is not observed on the application of other type of shear strain when the material is expanded in *x*-direction and compressed in *y*-direction (*xx*−*yy*) until 8−10%. In the former case, the delocalization of p_x-orbitals of chalcogenide atoms (see Figure 5) causes a shift in the position of VBM from L to M′ point, which mainly results in direct-to-indirect band gap transition. Moreover, an increase in the hybridization of $d_{xy}-d_{x^2-y^2}$ and d_{z^2} orbitals of metal shifts the CBM from L to a point between L and M′. In the latter case, the delocalization of p_y-orbitals is not observed and thus the nature of the band gap remains unchanged. The isosurface plots of charge density at chalcogenide atoms of MoX_2 when they are expanded in *x*/*y*-direction and compressed in *y*/*x*-direction (*xx*−*yy*/*yy*−*xx*) by 2%, 6%, and 10% are presented in Figure 5. It is evident from the figure that heavier chalcogenides are more diffuse. Also, the charge density is localized in case of MoS_2, while it gets delocalized in *x*-direction with the increase in strain when monolayers of $MoSe_2$ and $MoTe_2$ are compressed in *x*-direction and stretched in *y*-direction.

Next we discuss the quantitative variations in the band gap of TMDs exhibiting heavier chalcogenides.

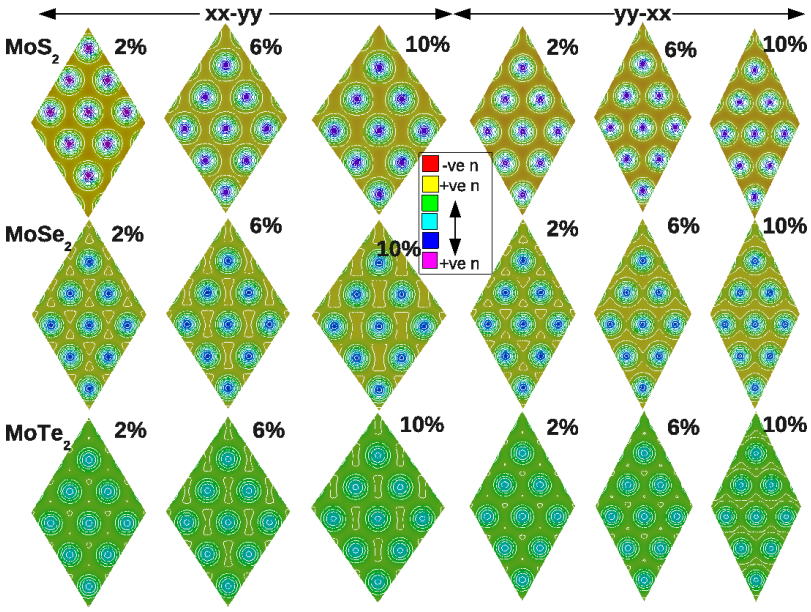

Figure 5. Isosurface plot of the charge density (*n*) of chalcogenide atoms of monolayer MoS_2 (top), $MoSe_2$ (middle), and $MoTe_2$ (bottom) when they are expanded along the *x*/*y*-direction and compressed along the *y*/*x*-direction (*xx*−*yy*/*yy*−*xx*) by 2%, 6%, and 10%. The isosurface value was taken as 0.05 e/Å^3.

On examining Figure 2 we find that similar to that of MS_2, the band gap decreases rapidly when MSe_2 and MTe_2 are stretched symmetrically in both *x*- and *y*-directions. However, due to the diffuse character of chalcogenide atoms larger strain is required on moving from MS_2 to MSe_2 to MTe_2 to attain semiconductor-to-metal transition. On the application of pure shear strain, TMDs possessing heavier chalcogenide atoms show different behavior as compared to MS_2 (see Figure 2). In MS_2, for both types of shear strains (*xx*−*yy* and *yy*−*xx*) the band gap decreases slowly as compared to tensile strains and almost with the same rate. In MSe_2 and MTe_2, however, a split/divergence in the curves (band gap *vs* strain) of both types of shear strains is observed, which increases with the size of chalcogenide (see Figure 2). It is evident from Figure 2 that in contrast to MS_2, the band gap decreases rapidly when the system is stretched in the *y*-direction and compressed in *x*-direction (*yy*−*xx*), as compared to the other case of pure shear strain (*xx*−*yy*). In the former case when the strain is more than 2−6%, the band gap becomes comparable to the value of asymmetrical uniaxial and symmetrical biaxial tensile strain in case of MSe_2 and MTe_2, respectively (see Figure 2). Thus, by expanding and compressing the monolayer of MTe_2 along *y*- and *x*-directions, respectively, its band gap decreases with a rate similar to that exhibited by the symmetrical biaxial tensile strain and attains a semiconductor-to-metal transition at roughly 10% of pure shear strain.

This rapid decrease in the band gap of TMDs having heavier chalcogenides results from the increase in the overlapping of p_x-orbitals. Moreover, $d_{xy}-d_{x^2-y^2}$ orbitals which solely describe the VBM and the hybridized $d_{xy}-d_{x^2-y^2}$ and d_{z^2} orbitals which constitute CBM, shift relatively fast toward the Fermi level and thus, also contribute into rapid decrease of band gap with the increase in pure shear strain (see Figure 4). This is contrary to the case of symmetrical biaxial tensile strain where the rapid decrease in the band gap and the subsequent semiconductor-to-metal transition is achieved due to transition between d_{z^2} orbitals. Thus, our results reveal different physical reasons for attaining the semiconductor-to-metal transition using symmetrical biaxial tensile strain and pure shear strain (*yy*−*xx*). Through our calculations we demonstrate that unlike graphene, semiconducting TMDs are significantly sensitive to almost all types of mechanical strain and their electronic properties can widely be tuned and controlled by applying strain through various approaches. Thus, we predict that these materials are not only potential alternatives to graphene but can also define a new range of tunable nanodevices.

CONCLUSIONS

We performed *ab initio* density functional theory based calculations to study the effect of mechanical strains on the electronic properties of the monolayer of semiconducting transition metal dichalcogenides. Our results elucidate the importance of strain engineering in controllably tuning the band gap of TMDs. More specifically, they underscore the significance of pure shear strain in tuning the band gap of heavier TMDs, suggesting that these materials are promising candidates for a wide range of nanodevices with tunable properties. Our results are summarized as follows: (i) While the electronic structure of TMDs is significantly affected by the size and the electronic configuration of

the chalcogenide atom, it retains its character upon variation of the metallic atoms. (ii) Semiconducting TMDs are quite sensitive to mechanical strains. In particular, both tensile and shear strain reduce the band gap. (iii) Upon application of biaxial tensile strain, the band gap decreases rapidly as compared to unaxial tensile strain, and attains a semiconductor-to-metal transition at a small strain of around 10% due to overlapping of d_{z^2} orbital at Fermi level. (iv) Tensile strain also transforms the monolayer of TMDs from direct-to-indirect band gap materials. This transition is achieved at a small strain of 1−2% in case of transition metal disulfides, which gradually increases upon transitioning from sulfides to selenides to tellurides. (v) Upon application of pure shear strain to MS_2, the band gap decreases slower and its nature remains unaffected. However, a significant variation in the band gap is seen when the pure shear strain is applied to the monolayers of MSe_2 and MTe_2. Specifically, when they are compressed along the *x*-direction and expanded along the *y*-direction, the in-plane p_x-orbitals of heavier chalcogenides delocalize and this leads to a direct-to-indirect band gap transition. Moreover, an increase in the overlapping of p_x-orbitals and shifting of $d_{xy}-d_{x^2-y^2}$ and hybridized d_{z^2} and $d_{xy}-d_{x^2-y^2}$ orbitals toward the Fermi level reduce the band gap with the increase in strain. Because of the diffuse nature of heavier calcogenides, the band gap decreases relatively faster for the case of MTe_2 and leads to a semiconductor-to-metal transition when a pure shear strain (*yy*−*xx*) of $\varepsilon \gtrsim 10\%$ is applied. Thus, our calculations illustrate that semiconductor-to-metal transition can be achieved at the presence of both homogeneous biaxial tensile strain and pure shear strain, through different physical mechanisms.

TABLE 1. Lattice Constants[a]

	a (Å)				
strain	*xx*	*yy*	*xx*+*yy*	*xx*−*yy*	*yy*−*xx*
		MoS_2 (a_0 = 3.18 Å)			
2%	3.20	3.23	3.24	3.15	3.21
4%	3.21	3.28	3.31	3.12	3.24
6%	3.23	3.32	3.37	3.09	3.28
8%	3.24	3.37	3.43	3.06	3.31
10%	3.26	3.42	3.50	3.03	3.35
		$MoSe_2$ (a_0 = 3.32 Å)			
2%	3.33	3.36	3.38	3.28	3.35
4%	3.35	3.41	3.45	3.25	3.38
6%	3.37	3.46	3.51	3.22	3.42
8%	3.38	3.51	3.58	3.19	3.45
10%	3.40	3.56	3.65	3.16	3.49
		$MoTe_2$ (a_0 = 3.55 Å)			
2%	3.56	3.60	3.62	3.51	3.58
4%	3.58	3.65	3.69	3.48	3.62
6%	3.60	3.70	3.76	3.44	3.66
8%	3.62	3.76	3.83	3.41	3.69
10%	3.64	3.81	3.90	3.38	3.74

[a] Lattice constants of MoS_2, $MoSe_2$, and $MoTe_2$ when the monolayers are expanded in *x*-direction (*xx*), *y*-direction (*yy*), both *x*- and *y*-directions (*xx*+*yy*), expanded in *x*- and compressed in *y*-direction (*xx*−*yy*), and expanded in *y*- and compressed in *x*-direction (*yy*−*xx*) by 2%, 4%, 6%, 8%, and 10%. a_0 represents the optimized lattice parameters of the unstrained monolayers. The corresponding lattice parameters for WX_2 were found similar to MoX_2, and therefore, not presented here.

COMPUTATIONAL DETAILS

In this work, we investigated the effect of strain on the electronic structure of monolayers of semiconducting TMDs, represented by MX_2, where M = Mo and W, and X = S, Se, and Te. All configurations possess hexagonal symmetry and belong to the $P6_3/mmc$ group. The electronic structure calculations of unstrained and strained monolayers of TMDs were performed using first-principles DFT based methodology, as implemented in the Vienna *ab-initio* simulation (VASP) package.[33,34] Projector-augmented-wave (PAW) potentials[35] were used to account electron-ion interactions, while the electron exchange-correlation interactions were treated using generalized gradient approximation (GGA) in the scheme of Perdew−Burke−Ernzerhof.[36] To obtain the unstrained configuration, atomic positions and lattice vectors were optimized using a conjugate gradient algorithm. In the case of strained geometries, the lattice vectors were varied with a fixed value to constitute the strained cell, and atoms were allowed to relax. Atomic relaxation was performed until the interatomic forces were less than 0.01 eV/Å, which was found sufficient to obtain relaxed parameters. A *k*-point sampling of 35 × 35 × 1 was used for the relaxation calculations, while a denser mesh of 45 × 45 × 1 was considered postrelaxation to generate density of states and charge densities. A plane wave cutoff of 400 eV was used for all the calculations, and a vacuum of approximately six layers was introduced to avoid interaction between periodic images of slabs in the *z*-direction.

To examine various configurations of strained cells, strain was applied to all TMDs in symmetrical as well as asymmetrical manners. Mainly, five different types of strain distributions were studied, which include: (i) expansion in *x*-direction (*xx*), (ii) expansion in *y*-direction (*yy*), (iii) homogeneous biaxial expansion in *x*- and *y*-directions (*xx*+*yy*), (iv) expansion in *x*-direction and compression in *y*-direction (*xx*−*yy*), and (v) compression in *x*-direction and expansion in *y*-direction (*yy*−*xx*) with the same magnitude of strain. The first three strain profiles correspond to tensile strain, while the latter two are the examples of pure shear strain. Except for the pure shear strain where the system is expanded in *x*-direction and compressed in *y*-direction, all types of strain profiles lead to increase in the lattice parameter as compared to its optimized value (see Table 1).

Conflict of Interest: The authors declare no competing financial interest.

Acknowledgment. The support of the Army Research Office through Contract W911NF-11-1-0171 is gratefully acknowledged. Computational support for this research was provided by Grant TG-PHY100022 and Grant TG-DMR090098 from the TeraGrid advanced support program, and the Center for Computation and Visualization at Brown University. P.J. thanks M. Stournara for critical reading of the manuscript.

REFERENCES AND NOTES

1. Liang, W. Y.; Cundy, S. L. Electron Energy Loss Studies of the Transition Metal Dichalcogenides. *Philos. Mag.* **1969**, *19*, 1031–1043.
2. Wilson, J. A.; Yoffe, A. D. The Transition Metal Dichalcogenides Discussion and Interpretation of the Observed Optical, Electrical and Structural Properties. *Adv. Phys.* **1969**, *18*, 193–335.
3. Lee, P. A. *Physics and Chemistry of Materials with Layered Structures: Optical and Electrical Properties*; Reidel: Dordrecht, The Netherlands, 1976.
4. Bromley, R. A.; Yoffe, A. D.; Murray, R. B. The Band Structures of Some Transition Metal Dichalcogenides. II. Group IVA; Octahedral Coordination. *J. Phys. C* **1972**, *5*, 759.
5. Kasowski, R. V. Band Structure of MoS_2 and NbS_2. *Phys. Rev. Lett.* **1973**, *30*, 1175.
6. Coehoorn, R.; Haas, C.; Dijkstra, J.; Flipse, C. J. F.; Groot, R. A. d.; Wold, A. Electronic Structure of $MoSe_2$, MoS_2, and WSe_2. I. Band-Structure Calculations and Photoelectron Spectroscopy. *Phys. Rev. B* **1987**, *35*, 6195–6202.
7. Feng, C.; Ma, J.; Li, H.; Zeng, R.; Guo, Z.; Liu, H. Synthesis of Molybdenum Disulfide (MoS_2) for Lithium in Battery Applications. *Mater. Res. Bull.* **2009**, *44*, 1811–1815.
8. Benameur, M. M.; Radisavljevic, B.; Heron, J. S.; Sahoo, S.; Berger, H.; Kis, A. Visibility of Dichalcogenide Nanolayers. *Nanotechnology* **2011**, *22*, 125706.
9. Coleman, J. N.; Lotya, M.; O'Neill, A.; Bergin, S. D.; King, P. J.; Khan, U.; Young, K.; Gaucher, A.; De, S.; Smith, R. J.; *et al.* Two-Dimensional Nanosheets Produced by Liquid Exfoliation of Layered Materials. *Science* **2011**, *331*, 568–571.
10. Lee, C.; Li, Q. Y.; Kalb, W.; Liu, X. Z.; Berger, H.; Carpick, R. W.; Hone, J. Frictional Characteristics of Atomically Thin Sheets. *Science* **2010**, *328*, 76–80.
11. Radisavljevic, B.; Radenovic, A.; Brivio, J.; Giacometti, V.; Kis, A. Single-Layer MoS_2 Transistors. *Nat. Nanotechnol.* **2011**, *6*, 147–150.
12. Johari, P.; Vivek, V. B. Tunable Dielectric Properties of Transition Metal Dichalcogenides. *ACS Nano* **2011**, *5*, 5903–5908.
13. Banerjee, W., S.; Richardson; Colemane, J.; Chatterjee, A. A New Three-Terminal Tunnel Device. *Electron Dev. Lett.* **1987**, *8*, 347–349.
14. Hankare, P. P.; Chate, P. A.; Delekar, S. D.; Bhuse, V. M.; Asabe, M. R.; Jadhav, B. V.; Garadkar, K. M. Structural and Opto-electrical Properties of Molybdenum Diselenide Thin Films Deposited by Chemical Bath Method. *J. Cryst. Growth* **2006**, *291*, 40–44.
15. Tenne, R.; Wold, A. Passivation of Recombination Centers in *n*-WSe_2 Yields High Efficiency (Greater than 14%) Photoelectrochemical Cell. *Appl. Phys. Lett.* **1985**, *47*, 707–709.
16. Vellinga, M.; Jonge, R. d.; Haas, C. Semiconductor to Metal Transition in $MoTe_2$. *J. Solid State Chem.* **1970**, *2*, 299–302.
17. Boeker, R., Th.; Severin; Mueller, A.; Janowitz, C.; Manzke, R.; Vob, D.; Krueger, P.; Mazur, A.; Pollmann, J. Band Structure of MoS_2, $MoSe_2$, and α-$MoTe_2$: Angle-Resolved Photoelectron Spectroscopy and *ab Initio* Calculations. *Phys. Rev. B* **2001**, *64*, 235305.
18. Reshak, A. H.; Auluck, S. Band Structure and Optical Response 2H-MoX_2 Compounds (X = S, Se, and Te). *Phys. Rev. B* **2005**, *71*, 155114.
19. White, H. S.; Abruna, H. D.; Bard, A. J. Semiconductor Electrodes. *J. Electrochem. Soc.* **1982**, *129*, 265–271.
20. Ramasubramaniam, A.; Naveh, D.; Towe, E. Tunable Band Gaps in Bilayer Transition-Metal-Dichalcogenides. *J. Electrochem. Soc.* **2011**, *84*, 205325.
21. Guinea, F.; Katsnelson, M. I.; Geim, A. K. Energy Gaps and a Zero-Field Quantum Hall Effect in Graphene by Strain Engineering. *Nat. Phys.* **2010**, *6*, 30–33.
22. Ni, Z. H.; Yu, T.; Lu, Y. H.; Wang, Y. Y.; Feng, Y. P.; Shen, Z. X. Uniaxial Strain on Graphene: Raman Spectroscopy Study and Band-Gap Opening. *ACS Nano* **2008**, *11*, 2301–2305.
23. Cocco, G.; Cadelano, E.; Colombo, L. Gap Opening in Graphene by Shear Strain. *Phys. Rev. B* **2010**, *81*, 241412(R).
24. Choi, S.-. M.; Jhi, S.-. H.; Son, Y.-.W. Controlling Energy Gap of Bilayer Graphene by Strain. *Nano Lett.* **2010**, *10*, 3486–3489.
25. Pereira, V. M.; Neto, A. H. C.; Peres, N. M. R. Tight-Binding Approach to Uniaxial Strain in Graphene. *Phys. Rev. B* **2009**, *80*, 045401.
26. Kim, K. S. e. Large-Scale Pattern Growth of Graphene Films for Stretchable Transparent Electrodes. *Nature (London)* **2009**, *457*, 706–710.
27. Farjam, M.; Rai-Tabar, H. Comment on ″Band Structure Engineering of Graphene by Strain: First-Principles Calculations″. *Phys. Rev. B* **2009**, *80*, 167401.
28. Yun, W. S.; Han, S. W.; Hong, S. C.; Kim, I. G.; Lee, J. D. Thickness and Strain Effects on Electronic Structures of Transition Metal Dichalcogenedies: 2H-MX_2 Semiconductors (M = Mo, W; X = S, Se, Te). *Phys. Rev. B* **2012**, *85*, 033305.
29. Scalise, E.; Houssa, M.; Pourtois, G.; Afanas'ev, V.; Stesmans, A. Strain-Induced Semiconductor to Metal Transition in the Two-Dimensional Honeycomb Structure of MoS_2. *Nano Res.* **2012**, *5*, 43–48.
30. Mak, K. F.; Lee, C.; Hone, J.; Shan, J.; Heinz, T. F. Atomically Thin MoS(2): A New Direct-Gap Semiconductor. *Phys. Rev. Lett.* **2010**, *105*, 136805.
31. Kuc, A.; Zibouche, N.; Heine, T. Influence of Quantum Confinement on the Electronic Structure of the Transition Metal Sulfide TS(2). *Phys. Rev. B* **2011**, *83*, 245213.
32. Ataca, C.; Ciraci, S. Functionalization of Single-Layer MoS_2 Honeycomb Structures. *J. Phys. Chem. C* **2011**, *115*, 13303–13311.
33. Kresse, G.; Furthmuller, J. Efficient Iterative Schemes for *ab Initio* Total-Energy Calculations Using a Plane-Wave Basis Set. *Phys. Rev. B* **1996**, *54*, 11169–11186.
34. Kresse, G.; Furthmuller, J. Efficiency of *ab Initio* Total Energy Calculations for Metals and Semiconductors Using a Plane-Wave Basis Set. *Comput. Mater. Sci.* **1996**, *6*, 15–50.
35. Kresse, G.; Joubert, D. From Ultrasoft Pseudopotentials to the Projector Augmented-Wave Method. *Phys. Rev. B* **1999**, *59*, 1758–1775.
36. Perdew, J. P.; Burke, K.; Ernzerhof, M. Generalized Gradient Approximation Made Simple. *Phys. Rev. Lett.* **1996**, *77*, 3865–3868.